A new method for computing quasi-local spin and other invariants on marginally trapped surfaces

2009 Class. Quantum Grav. 26 245008

(http://iopscience.iop.org/0264-9381/26/24/245008)

IOP PUBLISHING CLASSICAL AND QUANTUM GRAVITY

Class. Quantum Grav. **26** (2009) 245008 (20pp) doi:10.1088/0264-9381/26/24/245008

A new method for computing quasi-local spin and other invariants on marginally trapped surfaces

Michael Jasiulek

Max-Planck-Institut für Gravitationsphysik, Albert-Einstein-Institut, Golm, Germany

E-mail: michael.jasiulek@aei.mpg.de

Received 25 June 2009, in final form 23 October 2009
Published 24 November 2009
Online at stacks.iop.org/CQG/26/245008

Abstract

We accurately compute the scalar 2-curvature, Weyl scalars, associated quasi-local spin, mass and higher multipole moments on marginally trapped surfaces in numerical 3+1 simulations. To determine the quasi-local quantities, we introduce a new method which requires a set of invariant surface integrals, allowing for surface grids of a few hundred points only. The new technique circumvents solving the Killing equation and is also an alternative to approximate Killing vector fields. We apply the method to a perturbed non-axisymmetric black hole ringing down to Kerr and compare the quasi-local spin with other methods that use Killing vector fields, coordinate vector fields, quasi-normal ringing and properties of the Kerr metric on the surface. Interesting is the agreement with the spin of approximate Killing vector fields during the phase of perturbed axisymmetry. Additionally, we introduce a new coordinate transformation, adapting spherical coordinates to any two points on the sphere such as the two minima of the scalar 2-curvature on axisymmetric trapped surfaces.

PACS numbers: 04.25.Dm, 04.30.Db, 04.70.Bw, 95.30.Sf, 97.60.Lf

(Some figures in this article are in colour only in the electronic version)

1. Introduction

Numerical relativity has undergone a rapid development in the past few years. After the breakthrough of [1–3], stable long-term simulations of binary black hole (BBH) systems are common practice, besides waveform modeling, to study the close-to-merger spin precession [4, 5] or to model the final spin [6–10] of BBH inspirals [11–16]. Recently, extensive investigations have been done concerning the formation process and spin evolution of black holes with accretion disks [17, 18] appearing in fully relativistic simulations of binary neutron stars [19–21], mixed binaries [22–24], rotating neutron star collapse [25–28] and rotating supermassive star collapse [29–31].

In these cases, accurate numerical techniques to extract the spin of a BH in a gauge invariant manner are required. It is common to obtain a rough approximation of the spin

through the quasinormal mode oscillation extracted from the gravitational waveform after merger within black hole perturbation theory. Another approximation scheme is to integrate the radiated angular momentum contained in the gravitational radiation at 'large' coordinate spheres to draw conclusions about the remaining spin of the system given the initial data.

Other methods, as discussed in this paper, use the gauge invariant notation of an apparent horizon (AH) or in more general terms a marginally outer trapped surface (MOTS) which can be located on the spatial slices of the simulation. There gauge invariant spin and mass can be defined, if an axial Killing vector field (KVF) Φ^a is present, as in the case of Kerr. But opposed to the stationary case, the spacetime outside the horizon can be dynamical without spoiling the gauge invariance of these quantities [32–35]. The invariant quasi-local spin $J[\Phi^j]$ is given by the surface integral (Brown–York form)

$$J[\Phi^j] := -\frac{1}{8\pi} \oint_S \Phi^j K_{ij} s^i \mathrm{d}A, \tag{1.1}$$

where $\mathrm{d}A$ is the 2D area element, K_{ij} is the extrinsic curvature of the Cauchy slice and s^i is the outward-pointing surface normal on the MOTS denoted by S. In order to obtain Φ^j the 2D Killing equation has to be solved; if the axisymmetry is perturbed approximate KVFs (aKVFs) have to be computed [36–38], for applications in BBH simulations see [11, 16]. Sometimes, due to computational reasons, the effort of finding a KVF or aKVF is not done and coordinate vector fields are instead used to estimate $J[\Phi^j] \approx J\left[\Phi^j_{\mathrm{cv}}\right]$; see e.g. [4, 39]. Another common set of methods for determining the spin uses properties of the Kerr solution at the horizon, such as the proper length of the 'equatorial' circumference [40] or the extrema of the scalar 2-curvature [16].

In this paper we present a new, comparatively easy to implement algorithm, which is based on a multipole decomposition of the *rotational* Weyl scalar $\mathrm{Im}\,\Psi_2$ [41] in the framework of the isolated and dynamical horizon formalism [33–35]; for reviews see e.g. [34, 42, 43]. The dipole term reads

$$J_1 = -\sqrt{\frac{1}{12\pi}} \frac{A}{4\pi} \oint_S \mathrm{Im}\,\Psi_2\, Y^{10}(\chi)\, \mathrm{d}A, \tag{1.2}$$

where A is the horizon area, (χ, ϕ) is an invariant coordinate system [41] 'tied' to the axisymmetry, such that J_1 and $J[\Phi^j]$ are identical, and $Y^{10}(\chi)$ is the spherical harmonic $l = 1$, $m = 0$. We circumvent the use of invariant coordinates/KVFs and instead use the surface averages μ_n[1] of the scalar 2-curvature ${}^2\mathcal{R}$ and $\mathrm{Im}\,\Psi_2$ to obtain J_1 and higher multipole moments

$$\mu_n(\bullet) := \langle(\langle\bullet\rangle - \bullet)^n\rangle, \quad \langle\bullet\rangle := \frac{1}{A}\oint_S \bullet\, \mathrm{d}A, \tag{1.3}$$

which are well defined, even if the axisymmetry is perturbed and that allow us to benefit from exact numerical integration in order to reduce grid size and numerical error significantly. The invariant surface integrals $\mu_n({}^2\mathcal{R})$, $\mu_n(\mathrm{Im}\,\Psi_2)$ are related to the horizon spin, mass and higher multipole moments by algebraic systems of equations. In principal, μ_n allow us to generalize the horizon multipole moments through solutions of these systems in the absence of axisymmetry.

In order to minimize the numerical error of $\mu_n({}^2\mathcal{R})$, $\mu_n(\mathrm{Im}\,\Psi_2)$ accurate numerical computations of the curvature components ${}^2\mathcal{R}$, $\mathrm{Im}\,\Psi_2$ and the surface triad[2] on the horizon are

[1] In statistics μ_n is called the nth *central moment* of the probability distribution of a random variable.

[2] Note that a 'coordinate-induced' surface triad on 'large' coordinate spheres (as for wave extraction via Ψ_4) can easily be computed analytically. On the other hand, the coordinate representation of the horizon is a deformed 2-sphere and the computation of derivatives delicate.

required. The horizon is usually given by $h(\theta, \phi) = \sqrt{\delta_{ij} X^i X^j}$, the Cartesian shape function, where X^j are the Cartesian coordinates at the 2-surface centered at a point inside. Instead of finite differencing, we expand the shape function in terms of a tensor basis to determine Cartesian derivatives off the surface, as commonly used in horizon finding algorithms [44]. But opposed to [44], we use another basis, which is easier to implement, and exact numerical integration to determine the multipole coefficients of $h(\theta, \phi)$, where [44] use minimization.

We apply the new method (in comparison with others) to the dynamical AH of a non-axisymmetric BH[3] ringing down to Kerr in a 3+1 simulation, where we follow the evolution of spin and mass multipoles until their final Kerr values are reached.

This paper is organized in the following way. In section 2, we briefly explain the numerical methods we use to compute KVFs and aKVFs on AHs. In section 3, we deduce formulae from the Kerr metric to determine Kerr spin and mass from the area and the 'equatorial' circumference or the extrema of the scalar 2-curvature on the horizon and give a new formula which requires the surface average $\mu_2({}^2\mathcal{R})$ and that we also apply to our simulations. In section 4, we show how to use the whole set of μ_n to extract the multipole spectrum of an axisymmetric isolated horizon. In section 5, we show how to compute the curvature components ${}^2\mathcal{R}$, Ψ_n and the surface triad accurately. In section 6, we explain the set-up and initial data of our 3+1 simulation. During the evolution we follow spin, mass and higher multipole moments, compare different methods to measure the spin and test their convergence. Notation: indices i, j, k indicate 3D Cartesian components, indices a, b, c label 2D components on the local horizon grid, letters l, m label spherical harmonics. We indicate dimensionless quantities (mass dimension) with a hat, e.g. $\hat{a} = a/m$, ${}^2\hat{\mathcal{R}} = {}^2\mathcal{R} \cdot A/(8\pi)$, $\mathrm{Im}\,\hat{\Psi}_2 = \mathrm{Im}\,\Psi_2 \cdot A/(4\pi)$.

2. Solving the 2D Killing equation numerically

The IH multipole moments are defined in an invariant coordinate system [41] which requires knowledge of the axial KVF on the horizon. Our approach does not explicitly require the KVF to extract the IH multipole moments and circumvents the invariant coordinates by using the surface averages $\mu_n({}^2\hat{\mathcal{R}})$, $\mu_n(\mathrm{Im}\,\hat{\Psi}_2)$ which can easily be computed in any coordinate system. Nevertheless, in the numerical simulation of section 6 we want to compare our method and hence require the KVF. Therefore, we will briefly explain the techniques we use to solve/approximate the Killing equation.

The induced 2-metric q_{ab} of a spheroid S embedded into Euclidean space admits one rotational Killing vector field Φ^a which is a solution of the *Killing equation*

$$\mathcal{L}_\Phi q_{ab} = 2\,{}^2D_{(a}\Phi_{b)} = 0, \tag{2.1}$$

where ${}^2D$ is the induced covariant derivative on S. The vector field Φ^a is unique up to a constant. For Kerr $\Phi^a = \partial_\phi$, where ϕ is the Boyer–Lindquist coordinate, this constant is fixed such that integral curves have an affine length of 2π, thus $\phi \in [0; 2\pi]$.

2.1. Killing transport method

In order to solve the Killing equation, we apply the *Killing transport method* [37], appendix of [45], which is explained in this section.

The method can be roughly divided into three steps: (1) determine a single vector of the KVF at a point on an arbitrary loop on S, (2) spread this vector throughout the whole surface and (3) normalize the whole KVF by normalizing an arbitrary integral curve to have an affine

[3] We evolve *two puncture* initial data with an initially non-axisymmetric common horizon.

length of 2π. The first two steps require the *Killing transport equation*

$$c^a\, {}^2D_a\Phi_b = c^a L\, {}^2\varepsilon_{ab}$$
$$c^a\, {}^2D_a(L\, {}^2\varepsilon_{bc}) = c^a {}^2R^d{}_{cba}\Phi_d, \tag{2.2}$$

where ${}^2\varepsilon_{ab}$ denotes the Levi-Civita tensor and ${}^2R^d{}_{cba}$ denotes the 2D Riemann tensor. The first equation holds, since ${}^2D_{(a}\Phi_{b)} = 0$ if Φ_b is a KVF and since any 2-form on S can be expressed as $L\,{}^2\varepsilon_{ab}$, where L is a function. The second equation follows from the first; see [45] for details. Therefore (2.2) hold for a KVF Φ^a and the corresponding function L for any vector field c^a.

On the other hand, assume that Φ_b and L were unknown, pick a loop, e.g. the equator c_e ($\theta = \pi/2, \phi$), of a spherical coordinate system, pick a point, e.g. P ($\theta = \pi/2, \phi = 0$), and identify $c^a := \partial_\phi$,[4] then (2.2) becomes an ODE for the unknown $(\Phi_1(\phi), \Phi_2(\phi), L(\phi))$ along c_e. This defines a linear operator for 3-vectors at P. If we pick three arbitrary, linear independent initial vectors at P, transport (2.2) them along the loop to P, we obtain a 3×3 matrix presentation of this operator. Two components of its eigenvector are the KVF at P (step 1), the third is the auxiliary function L at P. Next this 3-vector is transported with (2.2) along coordinate lines all over S, setting $c^a = \partial_\phi$ or $c^a = \partial_\theta$ respectively (step 2), where the transportation equation (2.2) by construction 'conserves' the Killing property. The last step (step 3) is to normalize the KVF, where we have to solve the ODE $\partial_t\theta = \Phi^1(\theta, \phi)$, $\partial_t\phi = \Phi^2(\theta, \phi)$, Φ^a_0, where the initial vector Φ^a_0 is arbitrary, to obtain an integral curve and normalize such that the curve parameter $t \in [0; 2\pi]$.

2.2. *Approximate Killing vector fields*

If the spheroid S is slightly deformed, similar to the initial non-axisymmetric AH in our simulation, no exact solution of (2.1) exists. But one could try to find a 'best match' which minimizes a certain norm of the lhs of (2.1) on S. Such vector fields are often denoted as approximate Killing vector fields (aKVF). Opposed to KVFs there is no unique definition of aKVFs. Dreyer *et al* [37] could show that the Killing transport method is still applicable to yield a 'well matching' aKVF. But one has to be aware that the final vector field will no longer be independent of the particular loops of transportation, although this effect may be negligible for practical applications, e.g. [4, 7], if the departure from axisymmetry is 'small'. The method has also been used to determine aKVFs in binary black hole initial data; see Caudill *et al* [39].

We found it useful to adapt the coordinate system on the horizon before applying the Killing transport method such that the azimuthal transport revolves the minima of the scalar 2-curvature[5]; see appendix B. Another approach to finding an approximate Killing vector field has been given by [38]. They use a variational principle to minimize the 'non-symmetric' features of the vector field. A similar method can be found in the appendix of [46], for an application to a BBH simulation see [16]. Recently Beetle [47] has pointed out that Cook's [38] approach is closely related to an older proposal by Matzner [36], where the aKVF is the solution of an eigenvalue problem. An outstanding question is still the normalization of these aKVFs. An interesting new idea has been given in the appendix of [46], where the aKVF is normalized to a particular surface integral instead of a single integral curve.

In our approach these difficulties do not appear because no KVF/aKVF is explicitly required to represent the axisymmetry/perturbed axisymmetry. Instead we compute the invariant surface averages μ_n which exist in any case, and from those we compute the IH

[4] The resulting KVF is independent of the initial loop, initial point and curve parameter.

[5] A spheroid has two minima of the scalar 2-curvature which coincide with the minima of the KVF, given by the symmetry axis of the body.

multipole moments/*generalized* IH multipole moments through the algebraic system linking the two sets of invariants, section 4.1.

2.3. Coordinate vector fields

If the coordinates are conveniently adapted to the metric manifold, the coordinate vectors can automatically generate symmetries (if existing), such as the Boyer–Lindquist coordinate vectors ∂_t and ∂_ϕ in a Kerr spacetime. This is also the case for the *adapted spherical coordinates* $(\theta_{\rm asc}, \phi_{\rm asc})$, see appendix B, and the particular initial set-up we chose in our simulations[6]. Then the coordinate vector field,

$$\Phi^a_{\rm asc} = \partial_{\phi_{\rm asc}}, \tag{2.3}$$

is a good approximation to the KVF and we can estimate the spin $J[\Phi^j] \approx J\big[\Phi^j_{\rm asc}\big]$ with (1.1); see the application in section 6.

Similarly the authors of [4, 39] use the three rotational Killing vectors of Euclidean space in Cartesian coordinates

$$\Phi^{i[j]}_{\rm cc} = (x^k - C^k)\epsilon^{ij}{}_k, \qquad j = 1, 2, 3, \tag{2.4}$$

where $\epsilon^{ij}{}_p\delta^{pk} = \epsilon^{ijk}$ is the flat space Levi-Civita tensor and C^j is a point inside S, to define an Euclidean spin vector $\big(J\big[\Phi^{i[1]}_{\rm cc}\big], J\big[\Phi^{i[2]}_{\rm cc}\big], J\big[\Phi^{i[3]}_{\rm cc}\big]\big)$ and together with (1.1) to estimate $J[\Phi^i] \approx J\big[\Phi^i_{\rm cc}\big]$, where $J\big[\Phi^i_{\rm cc}\big]$ denotes the Euclidean norm of this vector which allows them to study the spin precession in a BBH inspiral and to estimate the final spin after merger. Referring to [4] this Euclidean spin vector reproduces the Bowen–York spin parameters of the conformally flat initial data and for the final black hole $\big|J[\Phi^j] - J\big[\Phi^j_{\rm cc}\big]\big| \ll 1$ as in our simulations.

3. Invariants of the horizon in Kerr

Before we go into details of how the surface averages μ_n are linked to the IH multipole moments in the next section 4, we want to recall that the mass $M^{\rm Kerr}_l$ and angular momentum $J^{\rm Kerr}_l$ multipole moments of Kerr $M^{\rm Kerr}_l + i\,J^{\rm Kerr}_l = m(i\,J/m)^l$ are uniquely given by Kerr spin J and mass m. In this section, we will review the analytic formulae necessary to extract Kerr spin and mass from an AH and give a new formula which we apply in our simulations.

In many numerical simulations, Kerr spin and mass (J, m) are computed from the 'equatorial' circumference[7] and the area $(L(c_e), A)$ of the BH surface; see [40]. A more recent approach is to use an extremum of the scalar 2-curvature and the area $({}^2\mathcal{R}_{\rm ext}, A)$; see [46]. Each of these invariant pairs uniquely determines a Kerr spacetime and is related to the other through the Kerr metric such that we are free to choose the numerically most convenient one. In order to benefit from exact numerical integration and to avoid interpolation on the horizon, we chose the invariants $(\mu_2({}^2\hat{\mathcal{R}}), A)$; see (1.3). The explicit algebraic expressions relating $J \leftrightarrow L(c_{\rm e}) \leftrightarrow {}^2\mathcal{R}_{\rm ext} \leftrightarrow \mu_2({}^2\hat{\mathcal{R}})$ $(\leftrightarrow \mu_2(\mathrm{Im}\,\hat{\Psi}_2))$ are derived in the following.

Any axisymmetric 2-metric q_{ab} can be put in the compact form

$$\mathrm{d}q^2 = \frac{A}{4\pi}\left(\frac{1}{f(\chi)}\,\mathrm{d}\chi^2 + f(\chi)\,\mathrm{d}\phi^2\right). \tag{3.1}$$

[6] In general, this is not the case and the correct solution of the Killing equation has to be found. In our case, coordinate vector fields are very useful for the comparison of section 6.

[7] This is the curve $c_{\rm e}$ along the maximum of ${}^2\mathcal{R}$ in Kerr.

For the 2-surface of a Kerr black hole $f(\chi)$, see [48], is given by

$$f(\chi) = \frac{1-\chi^2}{1-\hat{\beta}^2(1-\chi^2)}, \qquad \chi := \cos\theta, \tag{3.2}$$

where $\hat{\beta} \in [0; 1/\sqrt{2}]$ is called the *Kerr distortion parameter* and (θ, ϕ) are the Boyer–Lindquist spherical coordinates. The distortion parameter $\hat{\beta}$ is related to the more familiar dimensionless spin parameter $\hat{a} = a/m = J/m^2$ by

$$\hat{\beta}^2 = \frac{1}{2}\left(1 - \sqrt{1-\hat{a}^2}\right) = \frac{\hat{c}^2}{\hat{c}^2+1} \tag{3.3}$$

to Kerr spin J and mass m [8] by

$$J = \frac{A}{8\pi}\sqrt{\frac{1-\sqrt{1-\hat{a}^2}}{1+\sqrt{1-\hat{a}^2}}} = \frac{A}{8\pi}\frac{\hat{\beta}}{\sqrt{1-\hat{\beta}^2}} =: \frac{A}{8\pi}\,\hat{c}\,, \qquad m = \frac{1}{2}\sqrt{\frac{A}{4\pi(1-\hat{\beta}^2)}}. \tag{3.4}$$

Smarr [48] pointed out the analog of the surface of rotating material bodies to the black hole horizon, where the equatorial circumference increases as the body spins up. The equatorial circumference for the Kerr horizon is given by integrating (3.1) along the maximum of ${}^2\mathcal{R}$ which is the curve $(\chi = 0, \phi)$,

$$L(c_e) = \oint_0^{2\pi} \sqrt{\frac{A}{4\pi}\, f(\chi=0)}\, \mathrm{d}\phi = \sqrt{\frac{A\pi}{1-\hat{\beta}^2}} = 4\pi m. \tag{3.5}$$

For the numerical application in arbitrary coordinates this is practical, if the curve c_e is known to overlap with a coordinate line. If this is not the case, the extrema of ${}^2\mathcal{R}$ are an appealing alternative; see [16, 46]. The scalar 2-curvature of q_{ab} (3.1) is

$${}^2\mathcal{R} = -\frac{8\pi}{A}\frac{1}{2}f''(\chi) \quad \rightarrow \quad {}^2\hat{\mathcal{R}} = -\frac{1}{2}f''(\chi), \tag{3.6}$$

with extrema at $\chi_{\min} = 1; -1\,,\ \chi_{\max} = 0$. We obtain

$${}^2\hat{\mathcal{R}}_{\max} = \frac{1}{(1-\hat{\beta}^2)^2}\,, \qquad {}^2\hat{\mathcal{R}}_{\min} = 1 - 4\hat{\beta}^2. \tag{3.7}$$

3.1. An invariant surface integral in Kerr

If the scalar 2-curvature (or alternatively $\mathrm{Re}\,\Psi_2$, since $\mathrm{Re}\,\Psi_2 = -\frac{1}{4}\,{}^2\mathcal{R}$ for Kerr) has been computed on a finite grid, interpolation is required to obtain the extrema. This is not necessary if the following surface integrals are employed

$$\mu_2({}^2\hat{\mathcal{R}}) := \langle(\langle {}^2\hat{\mathcal{R}}\rangle - {}^2\hat{\mathcal{R}})^2\rangle, \qquad \langle {}^2\hat{\mathcal{R}}\rangle := \frac{1}{A}\oint_S {}^2\hat{\mathcal{R}}\,\mathrm{d}A. \tag{3.8}$$

Moreover, the numerical error of $\mu_2({}^2\hat{\mathcal{R}})$ benefits from averaging over all points on the grid and exact numerical integration can be used. With the normalization of (3.6) the average $\langle {}^2\hat{\mathcal{R}}\rangle_{\mathrm{grid}} = 1 + \epsilon_{\mathrm{num}}$, where ϵ_{num} is the numerical error, for any 2-metric computed on a finite grid on S according to the Gauss–Bonnet theorem. For Kerr the integral appearing in (3.8) is taken over a rational function in χ. We obtain

$$\mu_2({}^2\hat{\mathcal{R}}) = \frac{-15 - 70\hat{c}^2 + 128\hat{c}^4 + 70\hat{c}^6 + 15\hat{c}^8}{80(1+\hat{c}^2)} + \frac{3(1+\hat{c}^2)^4}{16}\frac{\arctan(\hat{c})}{\hat{c}}, \tag{3.9}$$

[8] For completeness, note that $m_{\mathrm{irr}} = R_{\mathrm{areal}}/2$ is the *irreducible mass* and $R_{\mathrm{areal}} = \sqrt{A/(4\pi)}$ is the *areal radius*.

where $\hat{c}$ is as defined in (3.4). In our simulations, we compute the surface average $\mu_2({}^2\hat{\mathcal{R}})$ numerically and solve (3.9) for the Kerr $\hat{c}$. Kerr spin and mass are then given by $J = A/(8\pi)\hat{c}$ and $m^2 = A(1+\hat{c}^2)/(16\pi)$ (3.4). For the numerical application in section 6 the Kerr spin deviates significantly from the IH spin during the initial phase but the 'non-Kerr' features are radiated during the evolution and finally vanish below the numerical error.

Note that we could similarly use any $\mu_n({}^2\hat{\mathcal{R}})$, $n > 2$ or $\mu_n(\mathrm{Im}\,\hat{\Psi}_2)$, $n > 1$ to compute $\hat{c}$ for Kerr. In that case $\mathrm{Im}\,\hat{\Psi}_2 = -\frac{1}{4}g''(\chi)$, $g(\chi) := \frac{(1+\hat{c}^2)^2}{\hat{c}(1+\hat{c}^2\chi^2)}$, see [49] and some algebra. It follows that $\mu_1(\mathrm{Im}\,\hat{\Psi}_2) = 0$ and $\mu_1(\chi \cdot \mathrm{Im}\,\hat{\Psi}_2) = \hat{c}$. The explicit appearance of the Boyer–Lindquist coordinate ($\chi = \cos\theta$) is inconvenient for the numerical application. For $\mu_2(\mathrm{Im}\,\hat{\Psi}_2)$ we obtain an expression similar to (3.9) which is $\mu_2(\mathrm{Im}\,\hat{\Psi}_2) = \frac{-15+170\hat{c}^2+112\hat{c}^4+70\hat{c}^6+15\hat{c}^8}{320(1+\hat{c}^2)} + \frac{3(1+\hat{c}^2)^4}{64}\frac{\arctan(\hat{c})}{\hat{c}}$. To extract more information than the Kerr $\hat{c}$ we have to consider the whole set of μ_n and follow the procedure explained in the following section.

4. Invariants of axisymmetric isolated horizons

For the calculations in the last section to be reasonable when applied to an AH found in a numerical simulation, we had to assume that the detected 2-surface was in a slice of Kerr. We relax this condition and allow the spacetime to be dynamical in the vicinity of the horizon which we assume to be an axisymmetric *isolated horizon* (IH) [32, 33]. On the horizon in Kerr all multipole moments are necessarily given by spin and mass, therefore higher moments contain no extra information. This is in general not the case on an axisymmetric IH, where an infinite set of independent multipole moments permits more complexity; see [41].

Ashtekar *et al* [41] exploit the axisymmetry to define an invariant coordinate system (χ, ϕ) for which the 2-metric has the form (3.1), ∂_ϕ is the KVF and the (zonal) harmonics $\{Y^{l0}(\chi)\}$ represent an orthonormal basis $\oint_S Y^{l0}(\chi)Y^{l'0}(\chi)\,\mathrm{d}A = \frac{A}{4\pi}\delta^{ll'}$ which they use to define the dimensionless IH mass $\hat{I}_l$ and angular momentum $\hat{L}_l$ multipole moments

$$\hat{I}_l := \oint_S \tfrac{1}{4}{}^2\mathcal{R}(\chi)Y^{l0}(\chi)\,\mathrm{d}A, \qquad \hat{L}_l := -\oint_S \mathrm{Im}\,\Psi_2(\chi)Y^{l0}(\chi)\,\mathrm{d}A. \tag{4.1}$$

$${}^2\mathcal{R}(\chi) = 4\cdot\frac{4\pi}{A}\sum_{l=0}^{\infty}\hat{I}_l Y^{l0}(\chi), \qquad \mathrm{Im}\,\Psi_2(\chi) = -\frac{4\pi}{A}\sum_{l=0}^{\infty}\hat{L}_l Y^{l0}(\chi). \tag{4.2}$$

On IHs without matter fields (like in Kerr) the Weyl scalar Ψ_2 is invariant and $\mathrm{Re}\,\Psi_2 = -\frac{1}{4}{}^2\mathcal{R}$.

Note that for Kerr $J\cdot 8\pi/A = \hat{c} = \sqrt{1/(3\pi)}\,\hat{L}_1$ and for an IH $J[\Phi^j]\cdot 8\pi/A = \sqrt{1/(3\pi)}\,\hat{L}_1$, where Φ^j is the KVF corresponding to (χ,ϕ) and $J[\Phi^j]$ given by (1.1). Therefore, the curvature component $\mathrm{Im}\,\Psi_2$ is sometimes called *rotational* Weyl scalar and the $\hat{L}_l$ *angular momentum* multipole moments all vanish in the absence of spin.

The invariants $\hat{I}_l$, $\hat{L}_l$ are subject to certain algebraic constraints such that $\hat{I}_0 = \sqrt{\pi}$ (Gauss–Bonnet) that the mass dipole $\hat{I}_1$ and the angular momentum monopole $\hat{L}_0$ vanish[9]. If the 2-metric (3.1) admits a reflection symmetry as for Kerr $f(\chi) = f(-\chi)$, see (3.2), all odd $\hat{I}_l$ and even $\hat{L}_l$ vanish, too.

4.1. The invariants μ_n on axisymmetric isolated horizons

In analogy with the method explained in section 3.1 for Kerr, where we gave the formula (3.8) to compute the Kerr $\hat{c}$ from the surface average $\mu_2({}^2\hat{\mathcal{R}})$, we would like to relate the invariants $\mu_n({}^2\hat{\mathcal{R}})$, $\mu_n(\mathrm{Im}\,\hat{\Psi}_2)$ (1.3), which are numerically easy to obtain in any coordinate system, to

[9] Therefore, the invariant coordinates are sometimes called 'center of mass frame' of the IH.

the IH multipole moments (4.1) which would require the invariant coordinates for a direct computation of the integrals (4.1) (as for example done in [50]).

We obtain the algebraic relations between $\mu_n({}^2\hat{\mathcal{R}})$, $\mu_n(\mathrm{Im}\,\hat{\Psi}_2)$ and $\hat{I}_n$, $\hat{L}_n$ by inserting (4.2) into (1.3)

$$\mu_n({}^2\hat{\mathcal{R}}) = \left\langle \left(1 - 2 \sum_{l=0}^{l^I_{\max}} \hat{I}_l \, Y^{l0}(\chi) \right)^n \right\rangle , \qquad n = 2, 3, \ldots, n^I_{\max}, \tag{4.3}$$

$$\mu_n(\mathrm{Im}\,\hat{\Psi}_2) = \left\langle \left(0 + \sum_{l=0}^{l^L_{\max}} \hat{L}_l \, Y^{l0}(\chi) \right)^n \right\rangle , \qquad n = 2, 3, \ldots, n^L_{\max}, \tag{4.4}$$

where we assume that ${}^2\hat{\mathcal{R}}$, $\mathrm{Im}\,\hat{\Psi}_2$ are given by finite sets of multipole moments up to $l^I_{\max}$, $l^L_{\max}$. We obtain[10]

$$\mu_n({}^2\hat{\mathcal{R}}) = \sum_{m=0}^{n} \binom{n}{m} (-2)^m \sum_{|K_{l_{\max}}|=m} \binom{m}{K_{l_{\max}}} (\hat{I}_-)^{K_{l_{\max}}} \langle (Y^{-0})^{K_{l_{\max}}} \rangle, \tag{4.5}$$

$$\mu_n(\mathrm{Im}\,\hat{\Psi}_2) = \sum_{|K_{l_{\max}}|=n} \binom{n}{K_{l_{\max}}} (\hat{L}_-)^{K_{l_{\max}}} \langle (Y^{-0})^{K_{l_{\max}}} \rangle, \qquad n = 2, 3, \ldots, n_{\max}, \tag{4.6}$$

where $K_{l_{\max}} = (k_1, k_2, \ldots, k_{l_{\max}})$ is a multi-index of length $l_{\max}$, $\binom{k}{k_1, k_2, \ldots}$ is the multinomial coefficient and $(\hat{I}_-)^{K_{l_{\max}}} \langle (Y^{-0})^{K_{l_{\max}}} \rangle = (\hat{I}_1)^{k_1} (\hat{I}_2)^{k_2} \cdots \langle (Y^{10})^{k_1} (Y^{20})^{k_2} \ldots \rangle$. The integers $n^I_{\max}, n^L_{\max}$ match the numbers of non-trivial $\hat{I}_n$, $\hat{L}_n$ given by the algebraic constraints mentioned earlier and $l^I_{\max}, l^L_{\max}$. The coefficients $\langle (Y^{-0})^{K_{l_{\max}}} \rangle$ are integrals over products of (zonal) spherical harmonics. They are given by the associated Clebsch–Gordan coefficients and higher order generalizations.

Consider the following example. In a simulation of a perturbed Kerr spacetime, we locate the AH and compute the surface integrals $\mu_n({}^2\hat{\mathcal{R}})$, $\mu_n(\mathrm{Im}\,\hat{\Psi}_2)$ (1.3) numerically to $n_{\max} = 6$ [11] to equate them with the rhs of (4.3), where we assume that the 2-surface is a cross-section of an IH with reflection and axisymmetric 2-metric. Then the algebraic systems (4.3), (4.4) become

$$\mu_n({}^2\hat{\mathcal{R}}) = \left\langle \left(1 - 2 \left(\sqrt{\pi} Y^{00} + \sum_{l=2,4,6,8} \hat{I}_l Y^{l0} \right) + \mathcal{O}_I \right)^n \right\rangle, \qquad n = 2, 3, 4, 5, 6 \tag{4.7}$$

$$\mu_n(\mathrm{Im}\,\hat{\Psi}_2) = \left\langle \left(\sum_{l=1,3} \hat{L}_l Y^{l0} + \mathcal{O}_L \right)^n \right\rangle, \qquad n = 2, 4, 6, \tag{4.8}$$

which we solve for $\hat{I}_2$, $\hat{I}_4$, $\hat{I}_6$, $\hat{I}_8$, $\mathcal{O}_I$ and $\hat{L}_1$, $\hat{L}_3$, $\mathcal{O}_L$, where $\mathcal{O}_I, \mathcal{O}_L$ are constants accounting for the truncation of the expansions. Since we simulate a perturbed Kerr spacetime, we pick the solution that is real and for which $-\hat{I}_2 > \hat{I}_4 > -\hat{I}_6 > \mathcal{O}_I$ and $\hat{L}_1 > -\hat{L}_3 > \mathcal{O}_L$ holds as for Kerr.

[10] Here the indices I , L in $l^I_{\max}$, $l^L_{\max}$, $n^I_{\max}$, $n^L_{\max}$ are omitted.

[11] Formally the solutions of the algebraic systems depend on $n_{\max}$. It determines the number of multipole moments we can resolve $l_{\max}$ and is limited by the numerical noise. In practice, the solution for lower $l_{\max}$ does not change as we go to higher $n_{\max}$.

In analogy with electrodynamics dimensionful factors can be added to attribute a physical interpretation to $\hat{I}_l$, $\hat{L}_l$; see [41]. To obtain the spin we need

$$J_1 = \sqrt{\frac{1}{12\pi}}\frac{A}{4\pi}\hat{L}_1. \tag{4.9}$$

The equation $J[\Phi^j] = J_1$ holds if Φ^j is the KVF corresponding to the invariant coordinates (χ, ϕ).

The surface integrals μ_n are well defined even in the absence of axisymmetry and allow us to extend the concept of IH multipole moments by adding the $m \neq 0$ harmonics in the expansions of ${}^2\hat{\mathcal{R}}$ and $\mathrm{Im}\,\hat{\Psi}_2$ on the rhs of (4.9). Nevertheless, for the evolution of the non-axisymmetric initial data studied in section 6, we assume that the contribution of odd/even mass/angular momentum multipole moments (reflection symmetry), higher harmonics as well as $m \neq 0$ harmonics is small and can be accounted for through $\mathcal{O}_I$, $\mathcal{O}_L$. We do not further investigate the possibility of generalized multipole moments. Our approach aims at numerical convenience and is flexible enough to extract, in principle, other invariants like the generalized multipole moments proposed by Owen [51] who considers the eigenfunctions of the intrinsic Laplacian on the horizon.

5. Accurate computation of ${}^2\mathcal{R}$, Ψ_2 on the AH

In this section, we will show how to compute the curvature components ${}^2\mathcal{R}$ and Ψ_2 accurately, where we assume that the 3+1 evolution variables[12] extrinsic 3-curvature K_{ij}, 3-metric γ_{ij} (together with $\partial_i K_{jk}$, $\partial_i \gamma_{jk}$, $\partial_i \partial_j \gamma_{kk'}$) and the horizon coordinate shape X^j are given on a Cartesian grid. The accurate calculation of curvature components on a deformed 2-sphere in a Cauchy slice is a common problem in numerical relativity which appears in horizon finding algorithms. Various methods have been tried to discretize the necessary spatial derivatives $\partial_j h$, $\partial_i \partial_j h$ by finite differencing, finite element, pseudo-spectral and spectral methods, using squared (θ, ϕ) grids or multipatch grids; for a review see [52]. Our approach is motivated by the work of [44]. There a spectral decomposition of the coordinate shape function $h(\theta, \phi)$ is being used to compute Cartesian derivatives. The first derivatives $\partial_j h$ are necessary to obtain a surface triad $\{s^i, u^j, v^k\}$ (required to compute the Weyl scalars) and the second derivatives $\partial_i \partial_j h$ to obtain the extrinsic 2-curvature ${}^2K_{ij}$ of S embedded into the Cauchy slice (additionally required to compute the scalar 2-curvature).

If we parametrize the AH with spherical coordinates, the embedding $X^j(\theta, \phi)$ into the Cartesian grid is

$$X^j(\theta, \phi) = h(\theta, \phi)\, n^j + C^j, \tag{5.1}$$

where C^j is a coordinate location inside the horizon (for example the coordinate centroid), n^j is the Cartesian radial unit vector $n^j = \frac{1}{r}x^j$, $r = \sqrt{\delta_{ij}x^i x^j}$ and x^j are Cartesian coordinates.

5.1. Spectral decomposition

To compute spatial derivatives one could decompose $h(\theta, \phi)$ into

$$h(\theta, \phi) = \sum_{l=0}^{l_{\max}} \sum_{m=l}^{-l} [h]^{lm} Y^{lm}(\theta, \phi), \tag{5.2}$$

[12] They can easily be assembled from the BSSN evolution variables.

where $[h]^{lm}$ are the expansion coefficients and Y^{lm} are the spherical harmonics. The evaluation of $\partial_j Y^{lm}(\theta, \phi)$ would require the Jacobian to transform between spherical and Cartesian coordinates. This is inconvenient for the numerical application, since the Jacobian is singular at the spherical coordinate poles.

Therefore, Baumgarte *et al* [44] take a tensor basis which is built of the radial unit vector $n^i(x^j) = x^j/r$ and is thus defined in Cartesian coordinates (and is easily parametrized with any other local coordinate system on the 2-surface, e.g. spherical $n^i(\theta, \phi) = (\sin\theta\cos\phi, \sin\theta\sin\phi, \cos\theta)$ or stereographic coordinates $n^j(u, v) = (2u, 2v, u^2 + v^2 - 1)/(1 + u^2 + v^2)$),

$$h = \sum_{l=0}^{l_{\max}} [h]^{K_l} N_{K_l}, \tag{5.3}$$

where K_l is again a multi-index of length l, $N_{K_l} = n_{k_1} n_{k_2} \cdots n_{k_l}$ is the vector product of unit vectors and the location-independent coefficients $[h]^{K_l}$ are symmetric tracefree tensors (STF), the notation is adapted from [53]. If the STFs are known, they can be translated to obtain the expansion (5.3), for how to $[h]^{lm} \leftrightarrow [h]^{K_l}$ see [44]. The partial derivative of the tensor product $\partial_j N_{K_l}$ consists of the derivatives $\partial_i n_j = (\delta_{ij} - n_i n_j)/r$. In detail the implementation of the STF tensors and its derivatives is a bit cumbersome but straightforward.

We use another basis of the harmonics instead $(\delta_{ij} n^i \mathcal{N}^j)^l$, where $\mathcal{N}^j$ is a constant complex Euclidean null vector $(\mathcal{N}_j \mathcal{N}^j) = 0$, $\mathcal{N}^j \neq 0$, see section 11.5.1, vol. II [54] or [55]. The expression $(n_j \mathcal{N}^j)^l$ is a homogeneous harmonic polynomial of Euclidean space of order l, therefore $\Delta_{\text{flat}}(n_j \mathcal{N}^j)^l = 0$. The radial vector n^j defines a restriction of the polynomial to the unit sphere $x^i x^j \delta_{ij} = 1$. It is known that such restrictions are eigenfunctions of the Laplacian of the induced metric (this applies to any embedding of S^2 into Euclidean space, e.g. an ellipsoid). On the unit sphere, this implies $\Delta_\circ (n_j \mathcal{N}^j)^l = l(l+1)(n_j \mathcal{N}^j)^l$, where $\Delta_\circ$ is the Laplacian of the standard spherical 2-metric. This holds for any null vector $\mathcal{N}^j$. In order to span each l-eigenspace of $\Delta_\circ$ with $2l + 1$ linear independent eigenfunctions, we define a list of null vectors

$$\mathcal{N}^j_{[lm]} = (\mathrm{i}\sin(m a_l), \mathrm{i}\cos(m a_l), 1), \qquad a_l = \frac{2\pi}{2l+1}, \quad m = -l, \ldots, l, \tag{5.4}$$

where the roots of unity have been used such that $\mathcal{N}^j_{[lm]}$ have the Euclidean norm $\mathcal{N}_j \mathcal{N}^j = -|\mathrm{e}^{\mathrm{i}\frac{2\pi m}{2l+1}}|^2 + 1$. Now we can define the new basis $\Phi^{lm} := \left(n_j \mathcal{N}^j_{[lm]}\right)^l$ and decompose h into

$$h = \sum_{l=0}^{l_{\max}} \sum_{m=l}^{-l} [h]^{lm}_{\mathcal{N}} \left(n_j \mathcal{N}^j_{[lm]}\right)^l. \tag{5.5}$$

Φ^{lm}, $m = -l, \ldots, l$ are not orthogonal in each l-eigenspace but across different eigenspaces. They are related to the standard basis by

$$Y^{lm} = B^{lm} \sum_{m'=-l}^{l} \Phi^{lm'} \mathrm{e}^{-\mathrm{i}\, m' m\, a_l}, \tag{5.6}$$

$$\Phi^{lm} = \frac{1}{2l+1} \sum_{m'=-l}^{l} \frac{Y^{lm'}}{B^{lm'}} \mathrm{e}^{\mathrm{i}\, m' m\, a_l},$$

$$B^{lm} = (-1)^m \frac{1}{l!} \sqrt{\frac{(l+m)!(l-m)!}{4\pi(2l+1)}}. \tag{5.7}$$

and we can transform the coefficients $[h]^{lm} \leftrightarrow [h]^{lm}_{\mathcal{N}}$. Derivatives of the new basis[13] are given by

$$\partial_k \Phi^{lm} = (n_j \mathcal{N}^j)^{l-1} l \, (\partial_k n_j \mathcal{N}^j) \tag{5.8}$$

$$\partial_k \Phi^{lm} = (n_j \mathcal{N}^j)^{l-1} l \, \frac{1}{r} (\mathcal{N}_k - n_k n_j \mathcal{N}^j), \tag{5.9}$$

and similarly for higher derivatives $\partial_i \partial_j \Phi^{lm}$.

5.2. Surface triad

Now we have the Cartesian derivatives $\partial_j h$, $\partial_j \partial_i h$ at hand and are able to compute the outward pointing surface normal $s^j = \gamma^{jk} s_k$

$$s_j = \lambda (n_j - \partial_j h), \qquad \lambda = 1/\sqrt{\gamma^{ij}(n_i - \partial_i h)(n_j - \partial_j h)}. \tag{5.10}$$

In order to complete the surface triad $\{s^i, u^j, v^k\}$, we set $u^j = \frac{1}{\sqrt{\gamma_{ik} \partial_\theta X^i \partial_\theta X^k}} \partial_\theta X^j$ and $v^k = \varepsilon^{ijk} s_i u_j$, where $\varepsilon^{ijk} = \|\gamma\|^{-1/2} [123]^{ijk}$ is the spatial Levi-Civita tensor and $[123]^{ijk}$ is the pure alternating symbol.

5.3. Extrinsic and intrinsic 2-curvature

The extrinsic 2-curvature ${}^2K_{ij}$ of S embedded into the Cauchy slice is given by

$${}^2K_{ij} = D_i s_j - s_i s^k D_k s_j, \tag{5.11}$$

where the second derivatives $\partial_j \partial_k h$ are required and the Christoffel symbols associated with the 3-metric to compute the 3-covariant derivative D_j. Then the intrinsic 2-curvature ${}^2\mathcal{R}$ is given by Gauss' *theorema egregium*

$${}^2\mathcal{R} = \mathcal{R} - 2R_{ij} s^i s^j + {}^2\mathcal{K}^2 - {}^2K^{ij} \, {}^2K_{ij}, \tag{5.12}$$

where ${}^2\mathcal{K} = {}^2K_{ij} q^{ij}$ and $q^{ij} = \gamma^{ij} - s^i s^j$ is the induced 2-metric in Cartesian components (also required to raise the indexes of ${}^2K_{ij}$ in the last summand on the rhs of (5.12)) and R_{ij}, $\mathcal{R}$ are the three-dimensional Ricci tensor and scalar.

5.4. Area element

The computation of surface integrals on the AH requires the area element $\mathrm{d}A = \sqrt{\det q_{ab}} \, \mathrm{d}\theta \, \mathrm{d}\phi$, where we need the induced 2-metric in local coordinates

$$q_{ab} = \partial_a X^j \partial_b X^k \gamma_{jk}. \tag{5.13}$$

Here X^j is as defined in (5.1); for an alternative see the appendix of [44].

5.5. Ψ_2 and other Weyl scalars

To obtain mass and angular momentum multipoles (4.1), an accurate computation of Ψ_2, given the 3+1 evolution variables, is required. Additionally, we want to follow the constraints $\Psi_0 = 0$ and $\Psi_1 = 0$ which hold for Kerr and on IHs [32] in the simulation of section 6. The *electric* E_{ij} and *magnetic* B_{ij} parts of the Weyl tensor C_{ijkl} w.r.t. time-like normal $\tilde{n}^\mu$ of the Cauchy slice are

$$E_{ij} \equiv -C_{ijkl} \tilde{n}^k \tilde{n}^l = -R_{ij} + K_i{}^k K_{kj} - \mathcal{K} K_{ij}, \tag{5.14}$$

[13] Here we omit the subscripts $\mathcal{N}^j_{[lm]} \to \mathcal{N}^j$ for simplicity.

$$B_{ij} \equiv - \star C_{ijkl}\tilde{n}^k\tilde{n}^l = -\varepsilon_i{}^{kl} D_k K_{lj}. \tag{5.15}$$

We further project E_{ij}, B_{ij} onto the surface triad $\{s^i, u^j, v^k\}$ and obtain the Weyl scalars, see [56, 57],

$$\Psi_2 = -\frac{1}{2}(E_{jk} - \mathrm{i}B_{jk})s^j s^k, \tag{5.16}$$

$$\Psi_0 = -(E_{jk} - \mathrm{i}B_{jk})m^j m^k, \tag{5.17}$$

$$\Psi_1 = -\frac{1}{\sqrt{2}}(E_{jk} - \mathrm{i}B_{jk})m^j s^k, \tag{5.18}$$

where $m^j = \frac{1}{\sqrt{2}}(u^j - \mathrm{i}v^j)$.

We monitor the dynamics of the AH during the evolution in section 6 by computing the dimensionless surface integrals

$$\hat{\psi}_0 = \oint_S |\Psi_0|\,\mathrm{d}A, \qquad \hat{\psi}_1 = \oint_S |\Psi_1|\,\mathrm{d}A, \qquad \hat{\psi}_2 = \left|\frac{1}{8\pi}\oint_S 4\mathrm{Re}\,\Psi_2\,\mathrm{d}A + 1\right|, \tag{5.19}$$

which vanish for a MOTS in a slice of Kerr or an IH.

6. Numerical evolution and initial data

In order to test and compare the new techniques, we applied them to the dynamical AH of a non-axisymmetric spinning BH in a 3+1 simulation ringing down to Kerr which has been carried out using the CCATIE code [11]. This is a 3D finite differencing code based on the Cactus Computational Toolkit [58]. The CCATIE code provides a collection of modules (*thorns*) which allow us to use *puncture initial data* [59] with the TwoPunctures thorn [60], to do time evolution using the BSSN evolution system [61–63], to set proper gauge conditions (where we used 1+log slicing and a hyperbolic gamma-driver condition stemming from [64] but with advection terms [11]), to successively refine the Cartesian mesh with several nested static boxes around the AH (where we used the Carpet AMR driver [65]) and to locate the horizon every few time steps during the evolution [66]. The horizon finding thorn provides the shape function $h(\theta, \phi)$ which is being used by a separate thorn to interpolate (fourth-order Lagrange) all necessary 3+1 evolution variables onto the spherical grid, to accurately compute the curvature components ${}^2\mathcal{R}$, $\mathrm{Im}\,\Psi_2$ at the horizon (see section 5) and, finally, to determine the associated quasi-local IH multipole moments using the surface integrals μ_n (1.3).

6.1. Initial data and grid parameters

In order to model the common horizon after the coalescence of an arbitrarily aligned BBH system, we chose as a non-trivial initial configuration a misaligned spinning puncture with a nearby smaller non-spinning companion puncture, where the common horizon is already present on the initial slice. The Bowen–York parameters of the first puncture are $m_1 = 0.8M$, $|s_1| = 0.3M^2$ with orientation ($\theta_{s_1} = 0.6$, $\phi_{s_1} = 0.4$) in the Cartesian grid. And for the second puncture we set $m_2 = 0.2M$, $s_2 = 0$.

The evolution is being carried out using the method of lines with the fourth-order Runge–Kutta time integrator and fourth-order centered stencils for spatial differentiation with the Cartesian grid resolutions $\Delta x = 0.048M$, $0.035M$, 0.025, $0.02M$ (finest AMR resolutions). To determine the KVF/aKVF, we use the Killing transport method (2.1) with second-order centered stencils for differentiation and a second-order Runge–Kutta integrator; see [37]

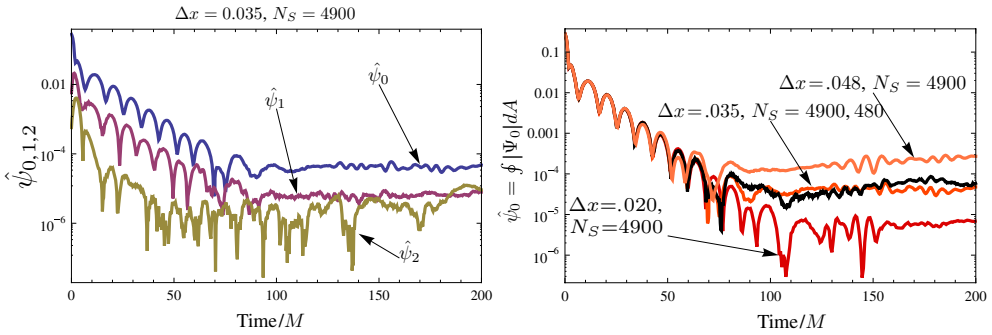

Figure 1. Left: time evolution of dimensionless surface averaged Weyl scalars $\hat{\psi}_{0,1,2}$. Right: time evolution of $\hat{\psi}_0$ for 3 different Cartesian resolutions.

for more details. To compute spatial derivatives of the shape function $h(\theta, \phi)$ we use its decomposition into spherical harmonics, where the spectral resolution is fixed at $l_{\max} = 10$. To compute the surface averages μ_n we use an exact integration scheme, see appendix A, and fix $n_{\max} = 6$. For every Cartesian resolution, we use three different spherical horizon grid resolutions $N_\theta \times N_\phi = N_S = 480,\ 1104,\ 4900$, where N_S is the total number of grid points on the surface and $N_\phi = 2(N_\theta + 1)$. The horizon finder is using a projective 6-patch grid [66] with approximately the same number of points as on the spherical grid.

6.2. Numerical evolution

6.2.1. Monitoring the isolation constraints To monitor the dynamics on the horizon, we computed the surface integrals (5.19) shown in figure 1 (for Kerr $\hat{\psi}_{0,1,2} = 0$). On the left, we see the typical exponentially damped oscillation of the *radiative* Weyl scalars Ψ_0, Ψ_1 which are (after an initial burst $\hat{\psi}_{0,1} \ll 1$) given by a superposition of several quasinormal-modes, predominately $l = 2$ modes, that have been excited by the specific initial data. As a fit to the ring-down profile of $\hat{\psi}_0$ we obtain the frequency $\omega_{\text{fit}} \approx 0.355 + 0.088\text{i}$, in agreement with the $l = 2$-mode frequencies $\omega_{l=2mn}$, see [67], which are $\omega_{2-20} \approx 0.34 + 0.089\text{i}$, $\omega_{220} \approx 0.36 + 0.089\text{i}$, ... for the case $J = 0.3$, $m = 1.035$. After around $t > 90M$ the perturbations are too weak to be further resolved limited by the total numerical error, which we downsize by increasing the Cartesian grid resolution, see figure 1 on the right, in order to see the dynamics below $\hat{\psi}_0 < 10^{-5}$. For $\Delta x = 0.035$ (black and orange) we computed $\hat{\psi}_0$ for two different spherical resolutions to show that the total error of $\hat{\psi}_0$ (and similar for surface integrals of other curvature components) is almost independent of the spherical resolution due to the spectral methods involved.

6.2.2. Evolution and convergence of the invariants μ_n. In figure 2, we see the exponentially damped oscillations of μ_n as they ring-down to their final Kerr value. On the right, it is shown how the time averages of $\mu_2({}^2\hat{\mathcal{R}})$ (120 M–200 M, straight black lines) converge with the expected fourth-order (4.01) as the Cartesian grid resolution increases after the oscillations have settled down. Apparently, the error of $\mu_2({}^2\hat{\mathcal{R}})$ does not converge uniformly but the effect flattens out as the Cartesian resolution increases.

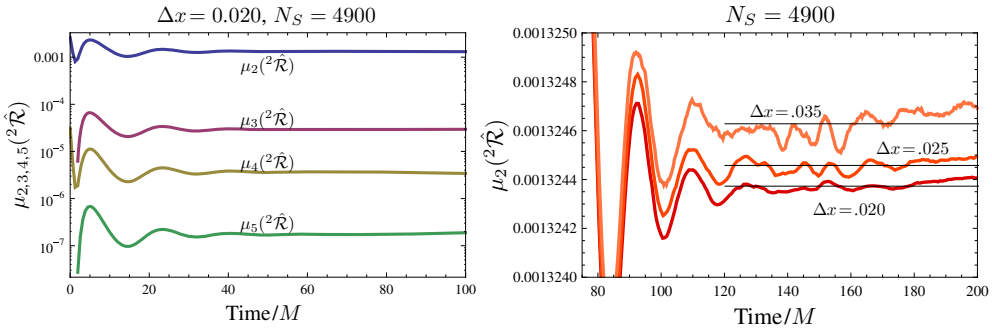

Figure 2. Left: time evolution of the surface averages $\mu_{2,3,4,5}(^2\hat{\mathcal{R}})$ over powers of the scalar curvature of the horizon. Right: time evolution of $\mu_2(^2\hat{\mathcal{R}})$ for three different Cartesian resolutions and time averages (straight lines) between 120 M and 200 M for each resolution.

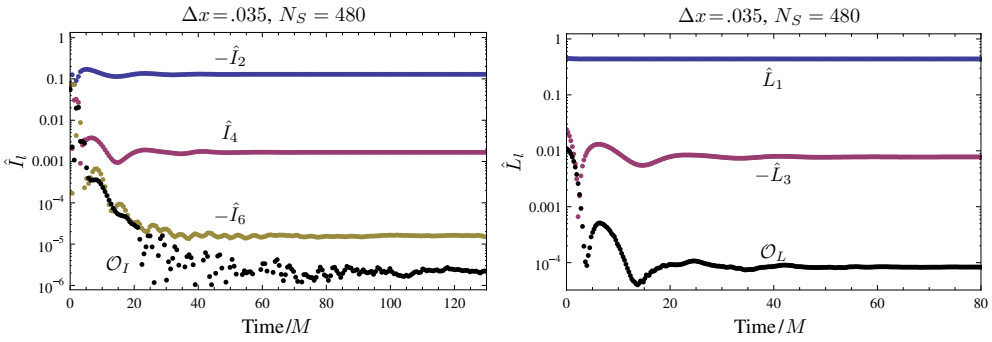

Figure 3. Left: time evolution of mass $\hat{I}_l$. Right: angular momentum multipole moments $\hat{L}_l$ given as a solution of the algebraic system (4.7) for μ_n up to $n_{\max} = 6$; $\mathcal{O}_I$, $\mathcal{O}_L$ account for all higher multipole moments.

6.2.3. Evolution of mass and angular momentum multipole moments. From μ_n we compute the IH multipole moments $\hat{I}_l$, $\hat{L}_l$ corresponding to a reflection axisymmetric horizon by solving the algebraic system (4.7), where $\mathcal{O}_I$, $\mathcal{O}_L$ account for all higher, non-axisymmetric and non-reflection symmetric multipole moments. It is apparent in figure 3 that these multipole moments are quickly radiated $t < 30$ M, leaving the horizon almost reflection axisymmetric but still oscillating. Interestingly, the dimensionless IH spin $\hat{L}_1$ is almost constant during the evolution, as is the horizon area (not plotted, $A \approx 4\pi \cdot 2.05^2 M^2$).

6.2.4. Spin evolution and comparison with other methods. In figure 4, we see the comparison between the various spin measures and their convergence. We have

(i) $J_1 = A/\sqrt{192\pi^3}\hat{L}_1$ (red) computed from μ_n, (4.7), assuming an axisymmetric IH,
(ii) $J[\Phi_{\rm kt}]$ (blue) computed from the Killing transport KVF/aKVF $\Phi_{\rm kt}$, (2.2), (1.1), assuming an axisymmetric IH,
(iii) $J[\Phi_{\rm cc}]$ (light green), $J[\Phi_{\rm asc}]$ (dark green) given by the coordinate vector fields $\Phi_{\rm cc}$ (Cartesian coordinates), (2.4), $\Phi_{\rm asc}$ (adapted spherical coordinates), (2.3), assuming 'small' coordinate distortions,
(iv) $J = J(\mu_2(^2\hat{\mathcal{R}}), A)$ (brown) computed from $\mu_2(^2\hat{\mathcal{R}})$, (3.8), assuming a Kerr horizon.

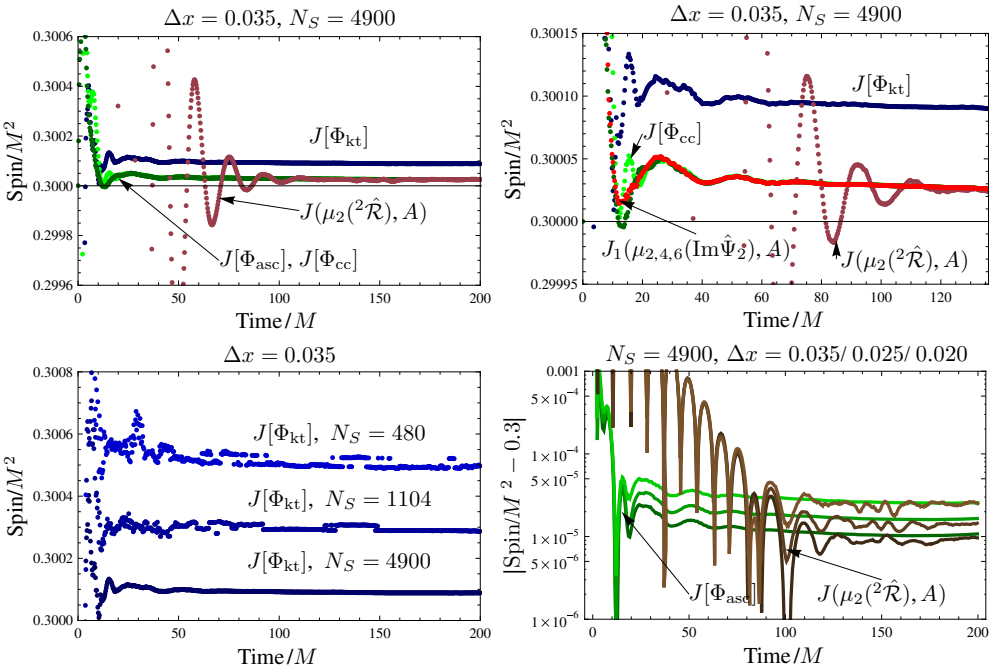

Figure 4. Top left: time evolution of spins given by the Killing transport aKVF $\Phi_{\rm kt}$, the coordinate vector fields $\Phi_{\rm asc}$, $\Phi_{\rm cc}$ and the Kerr spin computed from $\mu_2({}^2\hat{\mathcal{R}})$. Top right: zoom of 'top left' together with angular momentum dipole $J_1 = A/\sqrt{192\pi^3}\hat{L}_1$ (red) computed from μ_2, μ_4, μ_6 of $\mathrm{Im}\,\hat{\Psi}_2$. Bottom left: convergence of $J[\Phi_{\rm kt}]$ varying number of spherical grid points N_S. Bottom right: convergence of $J[\Phi_{\rm asc}]$, $J(\mu_2({}^2\hat{\mathcal{R}}), A)$ varying Cartesian resolution Δx.

After a short initial burst, all methods yield nearly the same spin value, which stays constant during the evolution; except $J(\mu_2({}^2\hat{\mathcal{R}}), A)$ (brown) which oscillates with the quasinormal frequency. During this phase the horizon seems to be best modeled assuming an axisymmetric dynamical horizon but not Kerr. We chose the numerical set-up such that the coordinate distortions are small and $J[\Phi_{\rm asc}]$, $J[\Phi_{\rm cc}]$ overlap with the invariant measure J_1. This is in general not the case in a full BBH simulation and these methods should be used with care.

In figure 4 (bottom right) we see the expected fourth-order convergence (w.r.t. Cartesian grid) of $J[\Phi_{\rm asc}]$, $J[\Phi_{\rm cc}]$ and $J(\mu_2({}^2\hat{\mathcal{R}}), A)$ toward $0.3M^2$. The convergence of J_1 is not shown explicitly. It is a smooth function of μ_n (convergence shown above) and converges therefore at the same rate. On the other hand $J[\Phi_{\rm kt}]$ converges at second order (w.r.t. the spherical grid), figure 4 (bottom left)[14], because the Killing transport method requires finite differencing on the horizon grid to determine $\Phi^j_{\rm kt}$.

7. Conclusion

The dominant part of the gravitational radiation at Scri is contained in the quadrupole moment of Ψ_4 which is in practice extracted at 'large' coordinate spheres around the source in

[14] Note that the low resolution $N_S = 480$ (light blue) is too coarse to be in the convergence regime.

numerical simulations. Similarly, the dipole moment of the rotational Weyl scalar $\mathrm{Im}\,\Psi_2$ encodes the quasi-local angular momentum measured at the apparent horizon in the presence of axisymmetry. The local coordinates on the horizon are in general distorted, and a solution of the Killing equation is required to determine an invariant coordinate system in which the multipole moments can be computed.

It is involved to determine the Killing vector field, in particular, to find a convenient approximant in case the axisymmetry is perturbed. We have shown a new method for extracting the horizon multipole moments using coordinate invariant surface integrals μ_n from which we deduce the multipole moments as a solution of an algebraic system. In the case of an axisymmetric IH, the angular momentum dipole J_1 is equal to the spin $J[\Phi]$ given by a solution of the Killing equation Φ^j in agreement with our simulations. Interestingly, the spin of the aKVF Φ_{kt} (given by the Killing transport method) and the angular momentum dipole moment $J_1(\mu_n(\mathrm{Im}\,\hat{\Psi}_2), A)$ (given by μ_n) agree even in the absence of axisymmetry.

There seems to be a dynamical phase of the horizon in which it is better modeled by an axisymmetric dynamical horizon and not with Kerr. Nevertheless, after the horizon is settled, the Kerr formula is valid. Then the computation of the Kerr spin using the surface average $\mu_2({}^2\hat{\mathcal{R}})$ (or $\mu_2(\mathrm{Im}\,\hat{\Psi}_2)$) is sensible and numerically more convenient than using the horizon circumference. The deviations from Kerr oscillate in agreement with black hole perturbation theory, until they are no more resolvable due to numerical errors. Then the dipole moment of the rotational Weyl scalar agrees with the Kerr spin, and μ_n take their final Kerr values.

We have shown how to use spectral methods, in a 3+1 finite differencing code, to accurately compute curvature components at the horizon and to extract spin and other multipole moments saving computational costs. These techniques, in particular, the non-standard basis of spherical harmonics and the exact integration scheme, should be considered for wave extraction on coordinate spheres or constant mean curvature spheres [68, 69].

Acknowledgments

I am pleased to acknowledge Badri Krishnan for his advice and fruitful ideas. I am grateful to Luciano Rezzolla, José Luis Jaramillo, Denis Pollney, Geoffrey Lovelace, Frank Ohme, Sascha Husa and Emma Robinson for helpful comments and discussions. I thank Erik Schnetter for providing the IsolatedHorizon thorn as the basis for my implementations. I also thank the anonymous referees for carefully reading the manuscript. Computations were performed at the LRZ Munich using the CCATIE code principally developed at the numerical relativity group at the AEI Potsdam. This work was supported by the Max Planck Society.

Appendix A. Exact integration schemes for spherical grids

It is well know that the equation

$$\int_a^b f(x)w(x)\,\mathrm{d}x = \sum_{i=1}^{N} w_i f(x_i) \tag{A.1}$$

holds exactly, where $w(x)$ is called the *weight function*, if $f(x)$ is a polynomial of degree less than $2N$ and the weights w_i and abscissas x_i are chosen in accordance with the orthogonal basis of polynomials on $[a, b]$ defined by the scalar product $\langle f|g\rangle := \int_a^b f(x)g(x)w(x)\,\mathrm{d}x$, because there are $2N$ degrees of freedom to make both sides of (A.1) match; see for example [70].

For the integration with $w(x) = 1$ on the circle $a = b$, the 'correct' weights and abscissas are particularly simple. They are N equi-distant points with equal weights. This cannot be generalized for the integration on the 2-sphere

$$\oint_{S^2} f(x, y)\, \mathrm{d}A = \sum_{i=1}^{N_S} w_i f(x_i, y_i), \tag{A.2}$$

for arbitrary N_S, because the number of uniform grid structures is finite $N_S = 4, 6, 8, 12, 20$, corresponding to the faces of the platonic solids. Since this is a 2D integration, we have $3N_S$ degrees of freedom in the sum on the rhs of (A.2) and $(l_{\max} + 1)^2$ spherical harmonics of degree $\leqslant l_{\max}$. This means if $f(x, y)$ was given by an expansion up to $l_{\max}$, we needed at least $N_S = (l_{\max} + 1)^2/3$ points to make (A.2) hold. Let us say $f(x)$ was given by an expansion of $(7 + 1)^2 - 4$ spherical harmonics, then the integration (A.2) on an icosahedral grid $N_S = 20$ with equal weights would be exact. There is an extensive body of work on the problem of optimal integration schemes for $N_S > 20$ (*cubature problem*); see for example [71].

There are less optimal compromises available, which require many more points than $(l_{\max} + 1)^2/3$, but which are defined on regular spherical (θ, ϕ) grids. For example the Gauss–Legendre/Gauss scheme, where the integration along each interval $[-1, 1]$, $[0; 2\pi]$ is a Gaussian quadrature

$$\oint_0^{2\pi} \int_{-1}^{1} f(\chi, \phi)\, \mathrm{d}\chi\, \mathrm{d}\phi = \sum_{i=1}^{N_\chi} \sum_{j=1}^{N_\phi} w_i^\chi w_j^\phi f(\chi_i, \phi_j), \tag{A.3}$$

where again $\chi = \cos\theta$, $N_S = N_\theta \times N_\phi$ and $N_\phi = 2N_\theta$.

As before the ϕ-integration is a Gaussian quadrature for $\phi_j = 2\pi(j - 1)/N_\phi$, $j = 1, \ldots, N_\phi$ and equal weights $w_j^\phi = 2\pi/N_\phi$, the χ-integration (in that case called the Gauss–Legendre quadrature) for χ_i being the roots of the Legendre polynomials (according to the weight function $w(\chi) = 1$). The corresponding weights w_i^χ can be found in, e.g., [72]. This method is exact for polynomials of degree less than $2N_\theta$ (less than $\sqrt{2N_S} < \sqrt{3N_S}$).

An alternative integration scheme has been found by [73][15]. There the integration grid is a standard equi-angular (θ, ϕ) grid, $\theta_j = (j - 1/2)\pi/N_\theta$ (staggered) and the computation of the roots of the Legendre polynomials is not necessary. The weights for even/odd N_θ are given by

$$w_j^\theta = 4/N_\theta \sum_{k=0}^{N_\theta/2-1} \frac{1}{2l + 1} \sin((2k + 1)\theta_j), \quad N_\theta \text{ even}, \tag{A.4}$$

$$w_j^\theta = 4/N_\theta \left(\frac{1}{2N_\theta} \sin(N_\theta \cdot \theta_j) + \sum_{k=0}^{(N_\theta-1)/2-1} \frac{1}{2l + 1} \sin((2k + 1)\theta_j) \right), \quad N_\theta \text{ odd}, \tag{A.5}$$

which allows for exact integration of harmonics of order less than $N_\theta/2$ (less than $\sqrt{1/8\ N_S} < \sqrt{2N_S} < \sqrt{3N_S}$). Then equation (A.3) becomes

$$\oint_0^{2\pi} \int_0^{\pi} f(\theta, \phi) \sin\theta\, \mathrm{d}\theta\, \mathrm{d}\phi = \sum_{i=1}^{N_\theta} \sum_{j=1}^{N_\phi} w_i^\theta w_j^\phi f(\theta_i, \phi_j) \sin\theta_j. \tag{A.6}$$

A small summarizing example: for the total of $N_S = 512$, $N_\theta \times N_\phi = 16 \times 32$ the cubature limit is at $39 \approx \sqrt{3 \cdot 512} = \sqrt{3N_S}$, for the Gauss/Gauss–Legendre scheme we get

[15] The authors make use of the fact that the points $\chi_j = \cos\theta_j$ (although not the zeros of the Legendre polynomials on $[1; -1]$) are the zeros of the Chebyshev polynomials of the first kind.

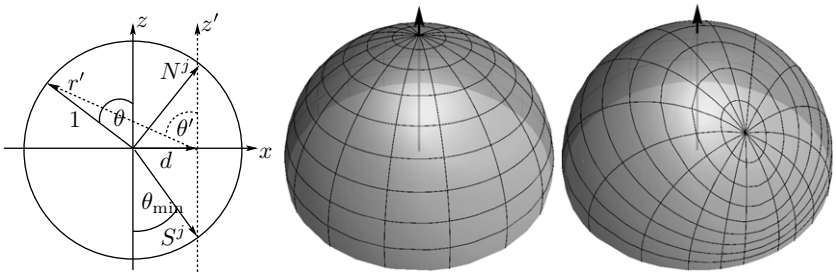

Figure B1. Parametrization of the unit-sphere with a shifted spherical coordinate system.

$l_{\max} < 32 = 2N_\theta$ and for the scheme of [73] we have $l_{\max} < 8 = N_\theta/2$ (we get almost the same limit on an icosahedral grid[16] with only $N_S = 20$, where $l_{\max} < 8 \approx \sqrt{3 \cdot 20}$).

Appendix B. Adapted spherical coordinates

Before solving the 2D Killing equation on a sphere, it is useful to have the 2-metric or the horizon shape in a convenient coordinate representation, which is 'roughly' adapted to the axisymmetry, such that the poles of the spherical coordinate system agree with the two minima of the scalar 2-curvature. We assume ${}^2\mathcal{R}(\theta, \phi)$ to be given on a spherical coordinate system (θ, ϕ), where the two minima are already in the xz-plane symmetric to the x-axis at $N^j = (\sin\theta_{\min}, 0, \cos\theta_{\min})$ and $S^j = (\sin\theta_{\min}, 0, -\cos\theta_{\min})$; see figure B1. This can always be accomplished by a simple Euler rotation.

In order to obtain the adapted spherical coordinates system (θ', ϕ'), we have to shift the Cartesian z-axis along the x-axis by the amount $d := \sin\theta_{\min}$. This is being done by

$$n_j(\theta, \phi) = r'(\theta', \phi')\, n'_j(\theta', \phi') + d \cdot (1, 0, 0), \tag{B.1}$$

where $n_j(\theta, \phi) = (\cos\phi \sin\theta, \sin\phi \sin\theta, \cos\theta)$, $n'_j(\theta', \phi') = (\cos\phi' \sin\theta', \sin\phi' \sin\theta', \cos\theta')$ are the radial unit vectors in the corresponding coordinate system. The distance $r'(\theta', \phi')$ is given by

$$r'(\theta', \phi') = \sqrt{d_\parallel^2 - 2 r_\parallel d_\parallel \sin\theta + r_\parallel^2}, \tag{B.2}$$

where $d_\parallel$, $r_\parallel$ are given by

$$r_\parallel = \cos\phi' \cos\phi + |\sin\phi'| \sqrt{1 - \cos^2\phi}, \tag{B.3}$$

$$d_\parallel = d \cos\phi'. \tag{B.4}$$

And finally, $\cos\phi$ and $\sin\theta$ in terms of θ', ϕ' are given by

$$\cos\phi = d \sin^2\phi' + \cos\phi' \sqrt{1 - d^2 \sin^2\phi'}, \tag{B.5}$$

$$\sin\theta = \frac{1}{r_\parallel} \left(d_\parallel \cos^2\theta' + \sin\theta' \sqrt{r_\parallel^2 - d^2 \cos^2\theta'} \right). \tag{B.6}$$

The inverse transformation is given by interchanging $\theta \leftrightarrow \theta'$, $\phi \leftrightarrow \phi'$ $d \leftrightarrow -d$ in the above expressions.

[16] Therefore, if one is only interested in the first coefficients of a smooth function on the sphere up to $l_{\max} = 6$, an icosahedral grid with equal weights would be a good choice.

References

[1] Pretorius F 2005 *Phys. Rev. Lett.* **95** 121101 (arXiv:gr-qc/0507014)
[2] Campanelli M, Lousto C O, Marronetti P and Zlochower Y 2006a *Phys. Rev. Lett.* **96** 111101 (arXiv:gr-qc/0511048)
[3] Baker J G, Centrella J, Choi D, Koppitz M and van Meter J 2006 *Phys. Rev.* D **73** 104002 (arXiv:gr-qc/0602026)
[4] Campanelli M, Lousto C O, Zlochower Y, Krishnan B and Merritt D 2007 *Phys. Rev.* D **75** 064030 (arXiv:gr-qc/0612076)
[5] Campanelli M, Lousto C O, Nakano H and Zlochower Y 2008 arXiv:0808.0713
[6] Rezzolla L *et al* 2008a *Astrophys. J.* **679** 1422 (arXiv:0708.3999)
[7] Rezzolla L *et al* 2008b *Astrophys. J.* **674** L29 (arXiv:0710.3345)
[8] Barausse E and Rezzolla L 2009 arXiv:0904.2577
[9] Tichy W and Marronetti P 2008 *Phys. Rev.* D **78** 081501 (arXiv:0807.2985)
[10] Boyle L and Kesden M 2008 *Phys. Rev.* D **78** 024017 (arXiv:0712.2819)
[11] Pollney D *et al* 2007 *Phys. Rev.* D **76** 124002 (arXiv:0707.2559 [gr-qc])
[12] Baker J G *et al* 2008 *Phys. Rev.* D **78** 044046 (arXiv:0805.1428)
[13] Herrmann F, Hinder I, Shoemaker D M, Laguna P and Matzner R A 2007 *Phys. Rev.* D **76** 084032 (arXiv:0706.2541)
[14] Marronetti P, Tichy W, Bruegmann B, Gonzalez J and Sperhake U 2008 *Phys. Rev.* D **77** 064010 (arXiv:0709.2160)
[15] Campanelli M, Lousto C O and Zlochower Y 2006b *Phys. Rev.* D **74** 084023 (arXiv:astro-ph/0608275)
[16] Scheel M A *et al* 2009 *Phys. Rev.* D **79** 024003 (arXiv:0810.1767)
[17] Kiuchi K, Sekiguchi Y, Shibata M and Taniguchi K 2009 arXiv:0904.4551
[18] Shibata M and Taniguchi K 2006 *Phys. Rev.* D **73** 064027 (arXiv:astro-ph/0603145)
[19] Shibata M 1999 *Prog. Theor. Phys.* **101** 1199 (arXiv:gr-qc/9905058)
[20] Font J 2008 *Living Rev. Rel.* **11** 86–91
[21] Baiotti L, Giacomazzo B and Rezzolla L 2008 *Phys. Rev.* D **78** 084033 (arXiv:0804.0594)
[22] Shibata M and Uryu K 2006 *Phys. Rev.* D **74** 121503 (arXiv:gr-qc/0612142)
[23] Etienne Z B *et al* 2008 *Phys. Rev.* D **77** 084002 (arXiv:0712.2460)
[24] Duez M D *et al* 2008 *Phys. Rev.* D **78** 104015 (arXiv:0809.0002)
[25] Shibata M 2003 *Phys. Rev.* D **67** 024033
[26] Shibata M, Baumgarte T W and Shapiro S L 2000 *Phys. Rev.* D **61** 044012
[27] Baiotti L *et al* 2005 *Phys. Rev.* D **71** 024035 (arXiv:gr-qc/0403029)
[28] Baiotti L and Rezzolla L 2006 *Phys. Rev. Lett.* **97** 141101 (arXiv:gr-qc/0608113)
[29] Saijo M, Baumgarte T W, Shapiro S L and Shibata M 2002 *Astrophys. J.* **569** 349 (arXiv:astro-ph/0202112)
[30] Shibata M and Shapiro S L 2002 *Astrophys. J.* **572** L39 (arXiv:astro-ph/0205091)
[31] Saijo M and Hawke I 2009 *Phys. Rev.* D **80** 064001 (arXiv:0908.3002)
[32] Ashtekar A, Fairhurst S and Krishnan B 2000 *Phys. Rev.* D **62** 104025 (arXiv:gr-qc/0005083)
[33] Ashtekar A, Beetle C and Lewandowski J 2001 *Phys. Rev.* D **64** 044016
[34] Ashtekar A and Krishnan B 2004 *Living Rev. Rel.* **7** 10 (arXiv:gr-qc/0407042)
[35] Ashtekar A and Krishnan B 2002 *Phys. Rev. Lett.* **89** 261101
[36] Matzner R 2003 *J. Math. Phys.* **9** 1657
[37] Dreyer O, Krishnan B, Shoemaker D and Schnetter E 2003 *Phys. Rev.* D **67** 024018 (arXiv:gr-qc/0206008)
[38] Cook G and Whiting B 2007 *Phys. Rev.* D **76** 41501
[39] Caudill M, Cook G, Grigsby J and Pfeiffer H 2006 *Phys. Rev.* D **74** 64011
[40] Smarr L 1973a *Phys. Rev.* D **7** 289
[41] Ashtekar A, Engle J, Pawlowski T and Van Den Broeck C 2004 *Class. Quantum Grav.* **21** 2549 (arXiv:gr-qc/0401114)
[42] Booth I 2005 *Can. J. Phys.* **83** 1073 (arXiv:gr-qc/0508107)
[43] Gourgoulhon E and Jaramillo J L 2006 *Phys. Rep.* **423** 159 (arXiv:gr-qc/0503113)
[44] Baumgarte T, Cook G, Scheel M, Shapiro S and Teukolsky S 1996 *Phys. Rev.* D **54** 4849
[45] Wald G 1984 *General Relativity* (Chicago, IL: University of Chicago Press)
[46] Lovelace G, Owen R, Pfeiffer H P and Chu T 2008 *Phys. Rev.* D **78** 084017 (arXiv:0805.4192)
[47] Beetle C 2008 arXiv:0808.1745
[48] Smarr L 1973b *Phys. Rev.* D **7** 289
[49] Chandrasekhar S 1983 *The Mathematical Theory of Black Holes* (Oxford: Oxford University Press)
[50] Vasset N, Novak J and Jaramillo J L 2009 *Phys. Rev.* D **79** 124010 (arXiv:0901.2052)
[51] Owen R 2009 arXiv:0907.0280

[52] Thornburg J 2007 *Living Rev. Rel.* http://www.livingreviews.org/lrr-2007-3
[53] Thorne K S 1980 *Rev. Mod. Phys.* **52** 299
[54] Project B M, Erdélyi A and Bateman H and E. U. O. of Naval Research 1953 *Higher Transcendental Functions* (New York: McGraw-Hill)
[55] Lachieze-Rey M 2004 *J. Phys. A: Math. Gen.* **37** 205
[56] Kelly B 2004 The May Project: The Newman–Penrose Scalars www.eng.uah.edu/∼jacksoa/literature/NPScalars.pdf
[57] Smarr L 1975 *PhD Thesis* Texas University, Austin
[58] Allen G, Benger W, Goodale T, Hege H, Lanfermann G, Merzky A, Radke T, Seidel E and Shalf J 2000 *Proc. 9th Int. Symp. High-Performance Distributed Computing* pp 253–60
[59] Brandt S and Bruegmann B 1997 *Phys. Rev. Lett.* **78** 3606 (arXiv:gr-qc/9703066)
[60] Ansorg M, Bruegmann B and Tichy W 2004 *Phys. Rev.* D **70** 064011 (arXiv:gr-qc/0404056)
[61] Nakamura T, Oohara K and Kojima Y 1987 *Prog. Theor. Phys. Suppl.* **90** 1
[62] Shibata M and Nakamura T 1995 *Phys. Rev.* D **52** 5428
[63] Baumgarte T W and Shapiro S L 1998 *Phys. Rev.* D **59** 024007 (arXiv:gr-qc/9810065)
[64] Alcubierre M *et al* 2003 *Phys. Rev.* D **67** 084023 (arXiv:gr-qc/0206072)
[65] Mesh Refinement with Carpet http://www.carpetcode.org
[66] Thornburg J 1996 *Phys. Rev.* D **54** 4899 (arXiv:gr-qc/9508014)
[67] Leaver E W 1985 *Proc. R. Soc. Lond.* A **402** 285
[68] Schnetter E 2003 *Class. Quantum Grav.* **20** 4719 (arXiv:gr-qc/0306006)
[69] Metzger J 2004 *Class. Quantum Grav.* **21** 4625 (arXiv:gr-qc/0408059)
[70] Szegö G 1939 *Orthogonal Polynomials* (New York: American Mathematical Society)
[71] Sobolev S 1974 *Introduction to the Theory of Cubature Formulae* (Moscow: NAUKA)
[72] Press W, Teukolsky S, Flannery B and Vetterling W 1990 *Numerical Recipes: FORTRAN* (New York: Cambridge University Press)
[73] Driscoll J and Healy D Jr 1994 *Adv. Appl. Math.* **15** 202